Journal of Alloys and Compounds 480 (2009) 279–285

Contents lists available at ScienceDirect

Journal of Alloys and Compounds

journal homepage: www.elsevier.com/locate/jallcom

Effect of the synthesis route on the microstructure and the reducibility of $LaCoO_3$

S. Ivanova [a], A. Senyshyn [b], E. Zhecheva [a], K. Tenchev [c], V. Nikolov [a], R. Stoyanova [a,*], H. Fuess [b]

[a] Institute of General and Inorganic Chemistry, Bulgarian Academy of Sciences, Sofia 1113, Bulgaria
[b] Darmstadt University of Technology, Institute of Materials Science, Structure Research, Petersenstr. 23, D-64287 Darmstadt, Germany
[c] Institute of Catalysis, Bulgarian Academy of Sciences, Sofia 1113, Bulgaria

ARTICLE INFO

Article history:
Received 10 December 2008
Received in revised form 17 February 2009
Accepted 21 February 2009
Available online 5 March 2009

Keywords:
Oxide materials
Sol–gel processes
Reduction
X-ray diffraction
SEM
Electron paramagnetic resonance

ABSTRACT

The effect of the synthesis route on the microstructure and reducibility of lanthanum cobaltates ($LaCoO_3$) perovskites was examined. Two synthesis methods were used: thermal decomposition of freeze-dried La–Co-citrates and the Pechini method. The crystal structure, morphology and defect structure of $LaCoO_3$ were characterized by XRD powder diffraction, TEM and SEM analyses and electron paramagnetic resonance spectroscopy. The reducibility was tested by thermal programmed reduction with hydrogen. The intermediate stage of reduction was determined by *ex situ* XRD experiments. $LaCoO_3$ powders obtained by the Pechini method were reduced relatively easier as $LaCoO_3$ obtained from freeze-dried citrates. The $LaCoO_3$ reduction yielded Co metal and La_2O_3 via the formation of oxygen deficient Brownmillerite-type $La_3Co_3O_8$ and $La_2Co_2O_5$ oxides. For $LaCoO_3$ obtained from freeze-dried citrates and annealed at higher temperatures, Co metal, in addition to oxygen deficient perovskites, was formed at the initial stage of the reduction. The different reducibility of $LaCoO_3$ obtained by the Pechini method and that from the freeze-dried citrates was discussed taking into account the formation of oxygen-deficient phases from the Brownmillerite and Ruddlesden–Popper series during the reduction.

1. Introduction

Lanthanum cobaltates ($LaCoO_3$) with a perovskite type structure are recognized as promising cathode materials for intermediate-temperature solid oxide fuel cells, as well as automotive exhaust catalysts [1–3]. The state-of-the-art research is mainly devoted to the improvement of the performance of $LaCoO_3$ by development of rational methods of synthesis that influences the morphology and microstructure. Among several synthesis procedures including solution-based and solid-state reactions [4–19], the most widely used method is the Pechini method [20]. This method is based on the mixing of La and Co ions at an atomic scale by the use of citric acid as a chelating agent and of ethylene glycol to form a polyester-type resin [8,9,21–23].

One of the factors determining the $LaCoO_3$ application is the mobility of lattice oxygen [24–26]. To evaluate this factor, temperature-programmed reduction with H_2 is often used as a fast screening method [24,25]. The reduction of $LaCoO_3$ has been controversially discussed. Some authors [27–29] propose a two step process via intermediate oxygen-deficient oxides before the final reduction to Co metal and La_2O_3. Other reports [30–33], however, suggest one-step reduction directly to Co metal based on XRD, IR and XPS evidence. Irrespective of the intensive studies on the mechanism of $LaCoO_3$ reduction, the relationship between the synthesis procedure and reducibility of $LaCoO_3$ has only been studied sporadically [34]. The examination of this relationship is further initiated by the fact that the synthesis procedure affects the microstructure of $LaCoO_3$ [35–39].

The present study is aimed at examining the effect of the synthesis route on the microstructure and reducibility of $LaCoO_3$. Two solution-based methods were used for the preparation of $LaCoO_3$. The first one is the Pechini method. The second one is based on the formation of mixed La–Co-citrate precursors by freeze-drying of the corresponding solutions. To analyse the effect of the organic component on the morphology of $LaCoO_3$, the same metal-to-citric acid ratio (La:Co:citric acid = 1:1:10) was used for both methods. Thermal properties of freeze-dried citrates and Pechini-type precursors were followed by DTA and TG analysis. Structural and morphological characterization was made by XRD powder diffraction, TEM and SEM analysis. Electron paramagnetic resonance (EPR) spectroscopy was used to analyze the defect structure of $LaCoO_3$. The reducibility was tested by thermal programmed reduction (TPR) with hydrogen. The intermediate study of reduction was determined by *ex situ* XRD experiments.

2. Experimental

Homogeneous La–Co-citrate precursors were obtained by freeze-drying and by a Pechini-type reaction. Lanthanum–cobalt citrates were prepared by adding a 5 M

* Corresponding author. Tel.: +359 2 9793915; fax: +359 2 8705024.
E-mail address: radstoy@svr.igic.bas.bg (R. Stoyanova).

0925-8388/$ – see front matter © 2009 Elsevier B.V. All rights reserved.
doi:10.1016/j.jallcom.2009.02.096

aqueous solution of citric acid (CA) to a suspension of $CoCO_3$ in aqueous solution of $La(NO_3)_3{\cdot}6H_2O$ (1 M La). The ratio between the components was La:Co:CA = 1:1:2 and 1:1:10, the La:Co ratio being carefully controlled. After stirring, a clear solution was obtained, which was diluted to 0.25 M La (Co). For the preparation of freeze-dried precursors this solution was frozen instantly with liquid nitrogen and dried under vacuum (20–30 mbars) at −20 °C in an Alpha-Christ Freeze-Dryer. For the precursors obtained by the Pechini-type reaction the La–Co–CA solution with La:Co:CA = 1:1:10 was heated up to ~90 °C and ethylene glycol (EG) was added (CA:EG = 1:4). The solution thus obtained was continuously stirred with a magnetic stirrer on a hot plate to remove the excess of water and to accomplish the polyesterification reaction. Prolonged heating produced a more and more viscous and bubbly pink mass. The thermal decomposition of the La–Co-precursors was achieved at 400 °C for 3 h in air. Thus obtained solid residue was annealed between 600 and 900 °C for 20 h in air, then cooled down to room temperature with a rate of 5°/min. For the sake of convenience, the samples were further on denoted as P-$LaCoO_3$ and FD-$LaCoO_3$ for oxides derived from Pechini-type precursors and from freeze-dried citrates, respectively.

$LaCoO_3$ samples were also obtained by a conventional solid-state reaction between La_2O_3 and $CoCO_3$ at 800 and 900 °C for 20 h. The regime of thermal treatment of the latter samples was similar to that of the ex-citrate oxides.

The lanthanum and cobalt content of the initial salt used was determined complexometrically. The mean oxidation state of the cobalt ions in the $LaCoO_3$ samples was established iodometrically after dissolution of the powdered sample in HCl under argon.

X-ray structural analysis was made by a Bruker Advance 8 diffractometer with Cu Kα radiation. Step-scan recordings for structure refinement by the Rietveld method were carried out using 0.02°2θ steps of 5 s duration. The computer program FULLPROF was used in the calculations [40]. The crystallite size of oxides was calculated by the Scherrer equation from the line width of the (0 1 2) and (0 2 4) reflection peaks: $D_{hkl} = \lambda/((\beta^2 - \beta_o^2)^{1/2} \cos\theta_{hkl})$ where λ is Cu Kα radiation, β is the peak width at the half height corrected with instrumental broadening and θ_{hkl} is the Bragg angle. The line width was determined by profile analysis using a WinPlotr program.

The thermal analysis (simultaneously obtained DTA-, TG- and DTG-curves) of the precursors was carried out by a "Stanton Redcroft" apparatus in the temperature range up to 650 °C in air, a heating rate of 5 °C/min and sample mass of 10 mg.

The EPR spectra were recorded as the first derivative of the absorption signal of an ERS-220/Q spectrometer within the temperature range of 90–400 K. The g factors were determined with respect to a Mn^{2+}/ZnS standard. The signal intensity was established by double integration of the experimental EPR spectrum.

SEM images of powders coated with gold were obtained by a Zeiss DSM 962 microscope and by Philips XL30 scanning electron microscopes. TEM analysis was carried out with a Philips/FEI CM20 microscope, at an accelerating voltage of 200 kV.

Temperature programmed reduction experiments were carried out in the measurement cell of a differential scanning calorimeter (DSC), model DSC-111 (SETARAM), directly connected to a gas chromatograph (GC), in the 300–973 K range at a 10 K/min heating rate in a flow of Ar:H_2 = 9:1, the total flow rate being 20 ml/min. A cooling trap between DSC and GC removes the water obtained during the reduction. To obtain the *ex situ* XRD patterns of the partially reduced oxides, the reduction process was interrupted at selected temperatures and then the samples were cooled down to room temperature in an Ar:H_2 flow followed by Ar treatment for 10 min.

3. Results/discussions

3.1. Structural characterization of $LaCoO_3$

Fig. 1 compares TG, DTG and DTA curves of FD-$LaCoO_3$ and P-$LaCoO_3$. Both precursors have the same metal-to-citric acid ratio (1:1:10). As one can see, freeze-dried La–Co-citrates are decomposed at a lower temperature ($T \geq 120$ °C) in comparison to the Pechini-type precursors. There are two endothermic processes, at 135 and 170 °C, followed by exothermic processes at 323 and 343 °C. Based on the thermal properties of citrate complexes [41–44], the endothermic processes can be assigned to the dehydration and to the transformation of the citrate into aconitate, while the exothermic processes correspond to the combustion of the residual organics. In the presence of ethylene glycol, the citrate precursors are decomposed at a temperature higher than 250 °C. The higher temperature of thermal decomposition can be related to the esterification reaction between the citric acid and the ethylene glycol, which proceeds together with complexation of the metal ions by citric acid [23,45,46]. There are several exothermic peaks due to the vigorous combustion of the organics. The process is finished at 440 °C (a temperature higher than that of freeze-dried La–Co-citrates, 360 °C). Above 440 °C, a slight weight loss (about 1%) is

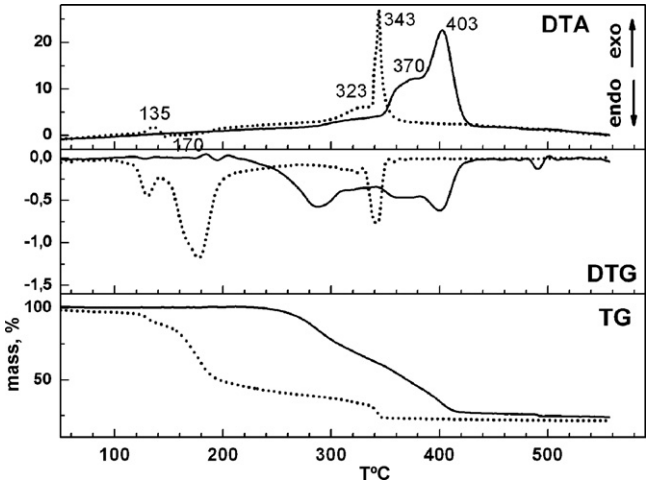

Fig. 1. TG, DTG and DTA curves of freeze-dried La–Co-citrate precursors (dotted line) and Pechini-type precursors (full line). The ratio between metal ions and citric acid is 1:1:10.

observed due to the burning of the deposed carbon. The same process of carbon burning is well established during thermal treatment of citrate complexes containing ethylene glycol [45,46].

At 400 °C and a heating time of 3 h, the product of thermal decomposition of both freeze-dried and Pechini-type precursors is a mixture of $LaCoO_3$, $La_2O_2CO_3$ and Co_3O_4 spinel (Fig. 2). This means that irrespective of the precursors used, the formation of $LaCoO_3$ proceeds by the interaction of $La_2O_2CO_3$ with the spinel oxide. It is worth mentioning that, at 400 °C, metastable cubic modification of $LaCoO_3$ is formed.

At 600 °C, a well-crystallized single phase of a rhombohedrally distorted $LaCoO_3$ perovskite was obtained by both methods (Fig. 3). In addition, the metal-to-citric acid ratio in the precursors did not affect the phase purity. Contrary to the metal-organic precursors, a solid-state reaction between La_2O_3 and $CoCO_3$ yielded single phase $LaCoO_3$ at $T \geq 800$ °C. Fig. 4 gives the unit cell parameters (a and c) and oxidation state of Co ions as a function of the preparation temperature for three series of samples: FD-$LaCoO_3$, P-$LaCoO_3$ and $LaCoO_3$ obtained by a solid-state reaction. Lattice parameters slightly change with the annealing temperature and are insensitive towards the synthesis route (Fig. 4). At 900 °C, all studied $LaCoO_3$ samples studied exhibited the identical lattice parameters, which coincide with those for $LaCoO_3$ reported in the literature [47,48]. The organic components of the precursors affect the oxi-

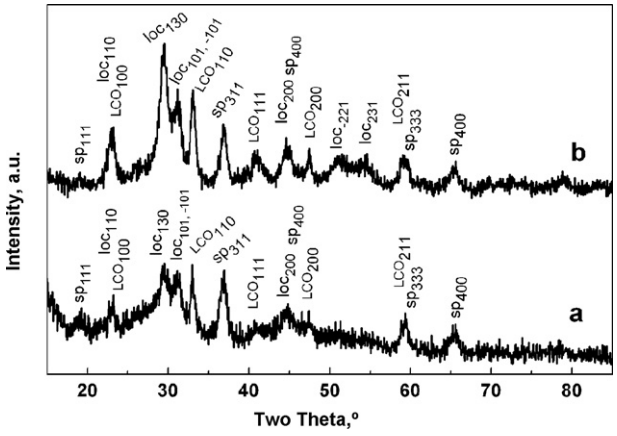

Fig. 2. XRD patterns of the thermal decomposition products of freeze-dried La–Co-citrates (a) and La–Co–CA–EG precursors (b) at 400 °C. Bragg reflections for cubic $LaCoO_3$ (LCO_{hkl}), monoclinic $La_2O_2CO_3$ (loc_{hkl}) and spinel phase (sp_{hkl}) are given.

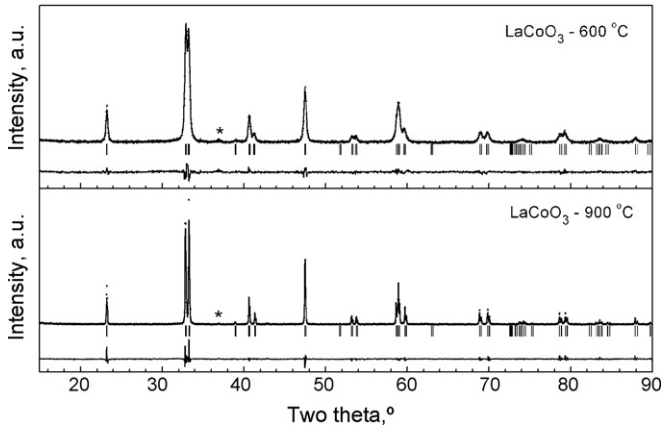

Fig. 3. XRD patterns of $LaCoO_3$ obtained from freeze-dried La–Co-citrates and annealed at 600 (upper curve) and 900 °C (lower curve) for 20 h. Asterisk denotes the impurity spinel phase.

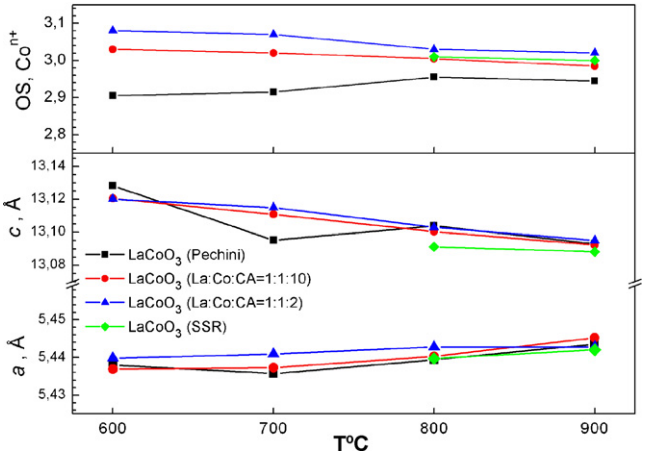

Fig. 4. Oxidation state of cobalt ions (OS, Co^{n+}) and unit cell parameters (a, c) for rhombohedrally distorted $LaCoO_3$ obtained from freeze-dried citrate precursors with metal-to-citric acid ratio 1:2 (triangle) and 1:10 (circle), by the method of Pechini (square) and by solid-state reaction (SSR, diamond). The annealing temperature varies between 600 and 900 °C.

dation state of Co ions. For FD-$LaCoO_3$ with La:Co:CA = 1:1:2, the oxidation state of Co ions is slightly higher than 3. By increasing the amount of the organic component, the oxidation state of Co decreases below 3 for P-$LaCoO_3$ reaching 3 for FD-$LaCoO_3$ with La:Co:CA = 1:1:10. The observed changes in the oxidation state of Co of $LaCoO_3$ samples imply different defect structures of the oxides depending on whether they are prepared from citrate or EG-citrate precursors.

EPR spectroscopy is a suitable experimental technique for monitoring the defect structure of $LaCoO_3$ and Ni-substituted $LaCoO_3$

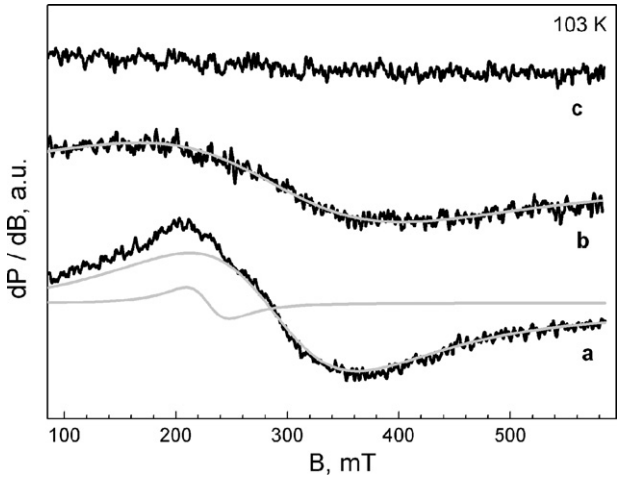

Fig. 5. EPR spectra at 103 K of $LaCoO_3$ annealed at 700 °C and obtained from freeze-dried La–Co-citrates with La:Co:CA = 1:1:2 (a) and La:Co:CA = 1:1:10 (b) ratio and by the method of Pechini (c). The black lines are the experimental spectra, while grey lines correspond to the simulated Lorentzian signals.

[34,38,39,49]. Thus, for $LaCoO_3$ prepared from freeze-dried citrates with a La:Co:CA ratio of 1:1:2, defects including ferromagnetic coupled Co^{3+} and Co^{4+} ions were detected by EPR [34]. These defects are located mostly on the interface between the primary particles which form aggregates [34]. Here, we are extending the EPR study to $LaCoO_3$ obtained from citrate and EG-citrate precursors with La:Co:CA = 1:1:10. Fig. 5 gives the EPR spectra of $LaCoO_3$ oxides annealed at 700 °C. It is worth mentioning that defectless $LaCoO_3$ does not give the EPR response in the X-band experiments (9.2 GHz) [34,38,39,49]. This picture is observed for P-$LaCoO_3$. Well-resolved EPR spectra are only observed for FD-$LaCoO_3$. The intensity of the EPR signals decreases with increasing Co-to-CA ratio. When $LaCoO_3$ is prepared from freeze-dried citrates with La:Co:CA = 1:1:2, the EPR spectrum consists of two overlapping signals having different line widths and g-factors: at 103 K the broader signal exhibits a line width of about 170 mT and a g-value of 2.8, while the line width of 40 mT and the g-value of 2.3 correspond to the narrower signal. Going to FD-$LaCoO_3$ with La:Co:CA = 1:1:10, only the broader signal becomes visible. According to our previous studies [34], both signals are due to the ferromagnetic ionic couples comprising Co^{3+} and Co^{4+} ions. It seems that the density of these defects is higher when $LaCoO_3$ is obtained from precursors containing lower contents of organics.

As in the case of the defect structure of $LaCoO_3$, the morphology of $LaCoO_3$ samples also depends on the synthesis procedure (Fig. 6). After decomposition of freeze-dried citrate precursors, plate-like aggregates are formed, their dimensions increasing with the decrease of the Co-to-CA ratio: from 5 to 20 μm to about 5 μm from oxides with La:Co:CA = 1:1:2 to oxides with La:Co:CA = 1:1:10. In comparison with freeze-dried citrate precursors, particles with

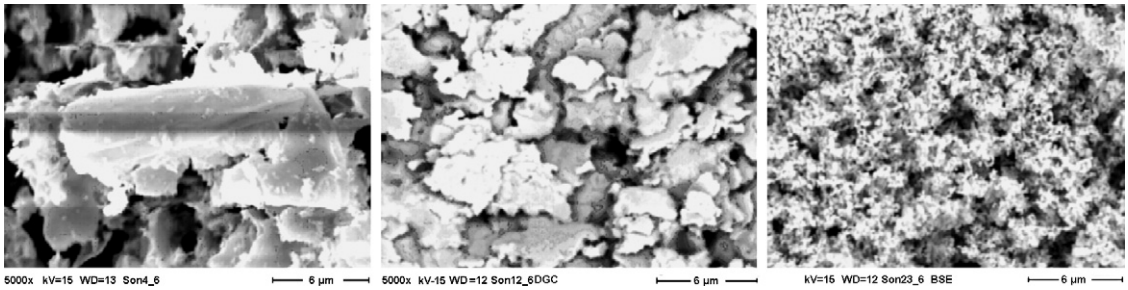

Fig. 6. SEM images of $LaCoO_3$ annealed at 600 °C and obtained from freeze-dried citrates with La:Co:CA = 1:1:2 (left), and 1:1:10 (centre) and by the method of Pechini (right).

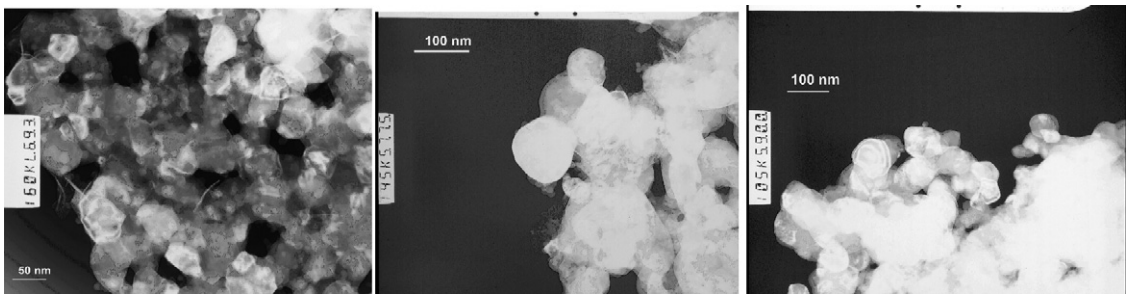

Fig. 7. TEM images of $LaCoO_3$ annealed at 600 °C and obtained from freeze-dried citrates with La:Co:CA = 1:1:2 (left), and 1:1:10 (centre) and by the method of Pechini (right).

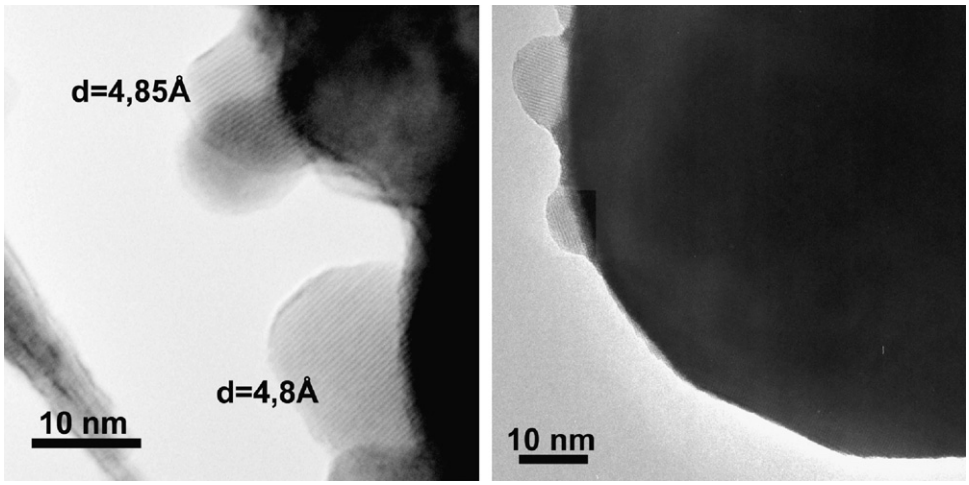

Fig. 8. HR-TEM images of $LaCoO_3$ annealed at 600 °C and obtained from freeze-dried citrates with La:Co:CA = 1:1:2 (left), and 1:1:10 (right). The value of the *d*-spacing is indicated.

a lower extent of agglomeration are formed by the Pechini method. The effect of the organic component in the precursors on the particle agglomeration of target $LaCoO_3$ can be related to their thermal behavior. It is noticeable that, for Pechini-type precursors, the carbon burning process takes place simultaneously with the formation of $LaCoO_3$.

Inside the aggregates, well-crystallized hexagonal individual particles become visible (Fig. 7). The particle dimensions fall in the nanometric scale and do not depend on the type of precursor used: 65 ± 15, 75 ± 15 and 80 ± 15 nm for FD-$LaCoO_3$ with La:Co:CA = 1:1:2, FD-$LaCoO_3$ with La:Co:CA = 1:1:10 and P-$LaCoO_3$. The insensitivity of particle dimensions is further supported by the crystallite sizes determined from the broadening of (0 1 2) and (0 2 4) diffraction lines: 40, 33 and 37 nm, respectively. It is important that the particle dimensions determined from TEM analysis match the crystallite sizes determined from diffraction line broadening, indicating the formation of nanometric crystallites of $LaCoO_3$.

The HR-TEM images show that impurity particles with dimensions of 10–15 nm are deposited on the surface of $LaCoO_3$ particles obtained from freeze-dried citrates only (Fig. 8). The lattice fingers correspond to *d*-values of about 4.80 and 4.85 Å. These *d*-values can be related to an impurity spinel phase with a lattice parameter of 8.40–8.45 Å. For the sake of comparison, the lattice parameter of the Co_3O_4 spinel is 8.08 Å. This indicates that the impurity cobalt spinel phase contains some La additives. (By a way of comparison, the ionic radii of octahedrally coordinated Co^{3+} (LS), Co^{2+} and La^{3+} ions are 0.525, 0.73 and 1.06 Å, respectively [50].) It is noticeable that impurity spinel phase is poorly visible in the XRD patterns of $LaCoO_3$ (the asterisk in Fig. 3).

By increasing the annealing temperature, the plate-like aggregates disappear leaving behind larger particles. At 800 °C, the

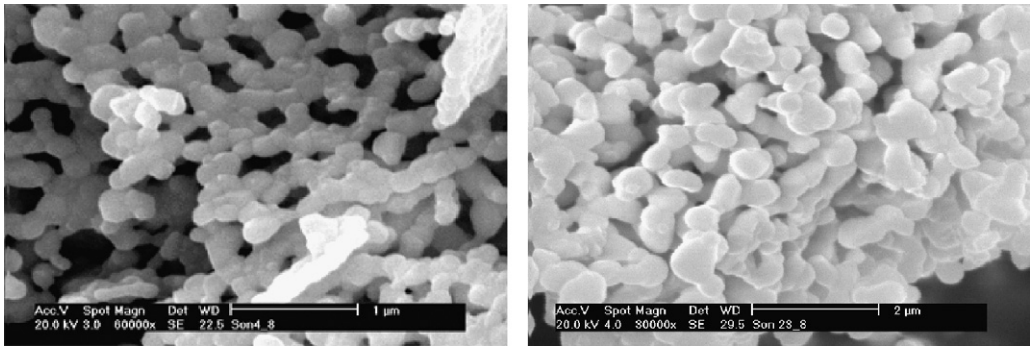

Fig. 9. SEM images of $LaCoO_3$ annealed at 800 °C and obtained from freeze-dried citrates with La:Co:CA = 1:1:10 (left) and by the method of Pechini (right).

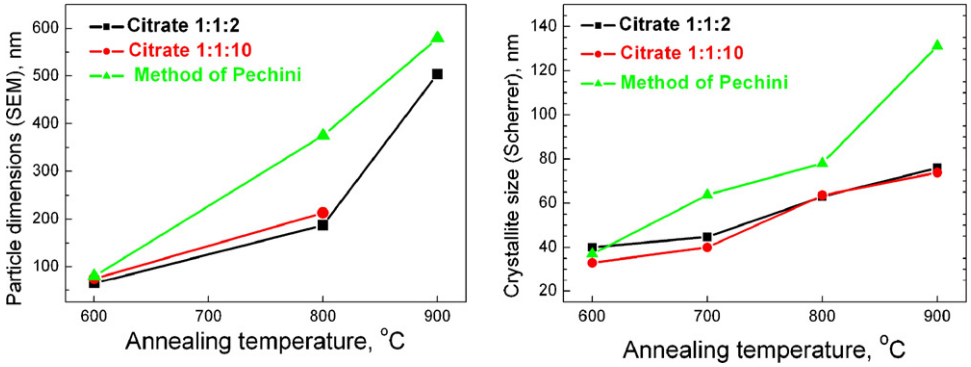

Fig. 10. Particle dimensions (determined from SEM analysis, left) and crystallite sizes (Scherrer size, right) of $LaCoO_3$ obtained from freeze-dried citrates with La:Co:CA = 1:1:2 (square) and 1:1:10 (circle) and by the method of Pechini (triangle) and annealed between 600 and 900 °C.

powders obtained from freeze-dried citrates are porous and show an uniform morphology with an open network of well shaped particles, while the Pechini method yields submicron particles loosely connected by each other (Fig. 9). Fig. 10 compares the particle growth process for oxides obtained by both methods. The particle dimensions and crystallite sizes were determined by SEM analysis and XRD line broadening. As one can see, FD-$LaCoO_3$ powders consist of smaller particles. The sintering process is easier for P-$LaCoO_3$ oxides. These results show that even at a higher annealing temperature (900 °C), the morphology of $LaCoO_3$ is still determined by the method of synthesis. The effect of the synthesis procedure on the morphology of $LaCoO_3$ has been reported for perovskites obtained by combustion, co-precipitation and citrate-gel methods [17,36].

3.2. Reducibility of $LaCoO_3$

Based on the structural, morphological and defects characterization of $LaCoO_3$ it is now possible to examine the reducibility of $LaCoO_3$. Fig. 11 compares the TPR curves of FD-$LaCoO_3$ and P-$LaCoO_3$. The TPR curves of all oxides studied display two well separated signals: the low-temperature signal (LT) developed between 300 and 500 °C and a high-temperature signal (HT) appearing above 500 °C. Table 1 gives the areas ratios of the HT-to-LT peaks. The peak areas were determined by numerical integration of the curves between 250 and 480 °C and between 480 and 700 °C for LT and HT peaks, respectively. As one can see, P-$LaCoO_3$ displays a lower reduction stability. For oxides annealed at 600 °C, the HT-to-LT area

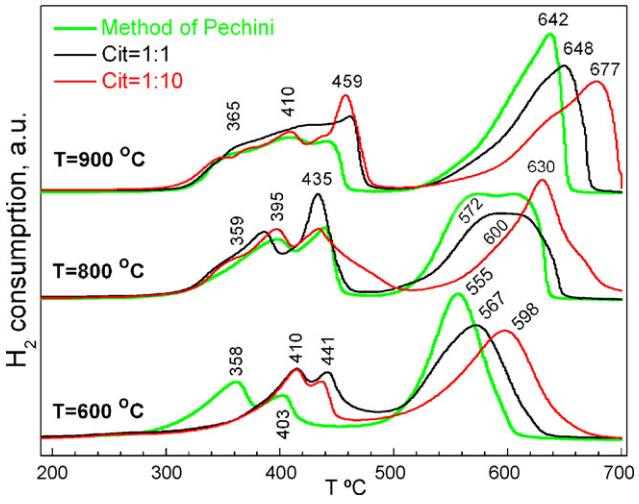

Fig. 11. TPR curves of $LaCoO_3$ annealed at 600, 800 and 900 °C and obtained from freeze-dried citrates with La:Co:CA = 1:1:2 and 1:1:10 and by the Pechini method.

ratio is close to 2 for P-$LaCoO_3$, while for FD-$LaCoO_3$ this ratio is slightly lower than 2. In addition, the LT reduction peak shows a complex structure as compared to the HT reduction peak. By increasing the annealing temperature, the LT reduction peak is spread in a wider temperature range and the HT reduction peak is shifted towards higher temperatures (Fig. 11). In the same sequence, the HT-to-LT area ratio decreases significantly (Table 1). This means that more Co ions are reduced in the low-temperature region. Of importance is that even at the highest annealing temperature used (900 °C), the area ratio for FD-$LaCoO_3$ remains lower in comparison to that for P-$LaCoO_3$.

To determine the products of $LaCoO_3$ reduction, *ex situ* XRD measurements of partially and completely reduced oxides were undertaken (Fig. 12). The reduced compositions were obtained after interruption of the reduction process at selected temperatures shown in Fig. 12. Taking into account the difference in $LaCoO_3$ reduction, two compositions were chosen: $LaCoO_3$ obtained by the Pechini method and annealed at 600 °C and $LaCoO_3$ derived from freeze-dried citrates and annealed at 900 °C. For P-$LaCoO_3$, the reduction up to 420 °C does not produce significant changes in the perovskite structure, while a mixture of Co metal and La_2O_3 is formed during the reduction up to 650 °C. At the initial stage of reduction of FD-$LaCoO_3$ (up to 420 °C), two distinct perovskite compositions from Brownmillerite series ($La_nCo_nO_{3n-1}$) were detected: $La_3Co_3O_8$ and $La_2Co_2O_5$. In the course of reduction (up to 490 °C), Co metal is formed in addition to the Brownmillerite-type oxides $La_nCo_nO_{3n-1}$. At high temperature (up to 695 °C), FD-$LaCoO_3$ is finally decomposed to Co metal and La_2O_3. Contrary to P-$LaCoO_3$, a La_2CoO_4 oxide from the Ruddlesden–Popper series ($La_{m+1}Co_mO_{3m+1}$) is also observed.

To rationalize the observed difference in reducibility of the $LaCoO_3$ oxides, the mechanism of interaction of $LaCoO_3$ with H_2 has to be taken into account. It has been proposed that the reduction of the cobalt ions in $LaCoO_3$ is a two-step process comprising the reduction of Co^{3+} ions to Co^0 metal via Co^{2+} ions [26–28]. At the first stage, there is a release of oxygen from the $LaCoO_3$ perovskite leading to the formation of perovskite-related phases from the Brownmillerite series where La-to-Co ratio is equal to 1 [51]. Above 500 °C, irreversible reduction of the oxygen deficient per-

Table 1
The high temperature (HT) to low temperature (LT) area ratio for $LaCoO_3$ as a function of the annealing temperature and the type of the precursors used.

Samples	T = 600 °C	T = 800 °C	T = 900 °C
La:Co:CA = 1:1:2	1.7	1.3	1.2
La:Co:CA = 1:1:10	1.9	1.1	1.1
Method of Pechini	2.0	1.8	1.7

The error of the determination is up to 10%.

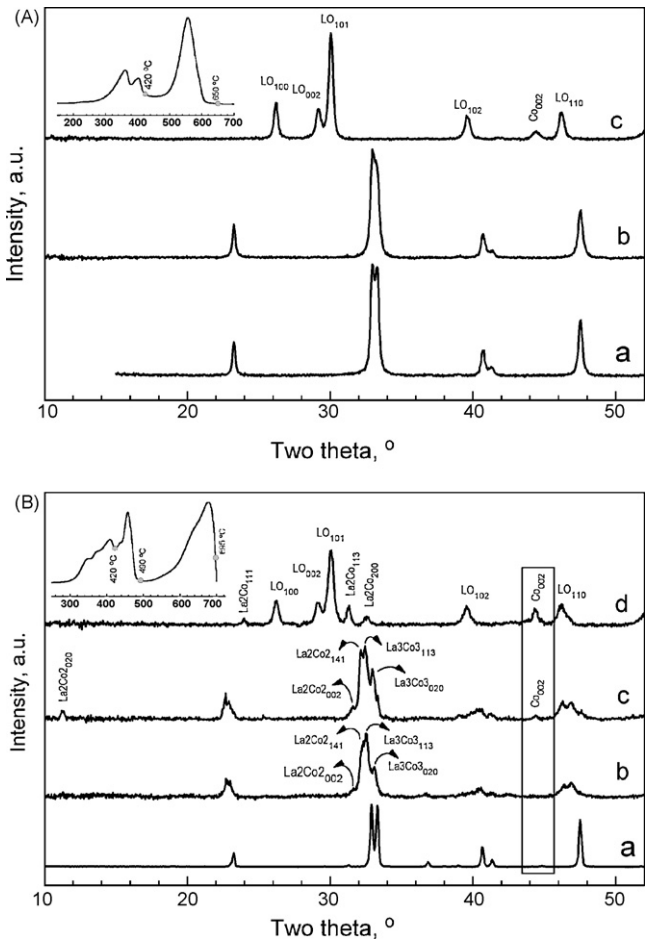

Fig. 12. XRD patterns of partially reduced oxides derived from P-$LaCoO_3$ annealed at 600 °C (A, a) and FD-$LaCoO_3$ annealed at 900 °C (B, a). The temperature where the reduction process is interrupted is shown in inset: 420 °C (A, b) and 650 °C (A, c) for P-$LaCoO_3$; and 435 °C (B, c), 490 °C (B, c) and 695 °C (B, d) for FD-$LaCoO_3$. Bragg reflections for $La_2Co_2O_5$ (La_2Co_{2hkl}), $La_3Co_3O_8$ (La_3Co_{3hkl}), La_2CoO_4 (La_2Co_{hkl}), La_2O_3 (LO_{hkl}) and Co metal (Co_{hkl}) are given. The inset shows the temperature where the reduction process is interrupted.

ovskites to cobalt metal and lanthanum oxide takes place. The two-step reduction process can be presented as [51–54]:

$$\text{Low-temperature peak}: LaCoO_3 + \tfrac{1}{2}H_2 \rightarrow \tfrac{1}{2}La_2Co_2O_5 + \tfrac{1}{2}H_2O \quad (1)$$

$$\text{High-temperature peak}: \tfrac{1}{2}La_2Co_2O_5 + H_2 \rightarrow \tfrac{1}{2}La_2O_3 + Co + H_2O \quad (2)$$

As the $LaCoO_3$ reduction proceeds by consecutive formation of Co^{2+} and Co^0 phases, the HT-to-LT area ratio has to be equal to 2.

However, based on X-ray photoelectron studies and magnetic measurements, the appearance of Co metal has been established in the low-temperature range [31,32]. This can be explained taking into account the instability of Brownmillerite-type oxides. In air, $La_nCo_nO_{3n-1}$ oxides with $n=2$ and $n=3$ accept rapidly oxygen, this leading to recovery of the initial $LaCoO_3$ phase [51]. In inert atmosphere, $La_nCo_nO_{3n-1}$ oxides are irreversibly decomposed to CoO and Ruddlesden–Popper phases $La_{m+1}Co_mO_{3m+1}$ [51,55]: $La_nCo_nO_{3n-1} \rightarrow n/(m+1)CoO + n/(m+1)La_{m+1}Co_mO_{3m+1}$, where the oxidation state of Co is preserved. Under the conditions of the TPR experiment, CoO is unstable and is easily reduced to Co metal (above 400 °C [56,57]). The proceeding of several concomitant reactions is the reason that the HT-to-LT area ratio is lower than 2 [34,58,59].

Returning to the samples studied by us, it is clear that two-step reduction of $LaCoO_3$ is accomplished only for oxides obtained by the Pechini method and annealed at 600 °C. The lack of detection of Brownmillerite-type oxides at the initial stage of reduction indicates that these phases are easily reoxidized to $LaCoO_3$ during the air exposure of the oxide for *ex situ* XRD experiments. In comparison with P-$LaCoO_3$, the re-oxidation of Brownmillerite-type oxides $La_nCo_nO_{3n-1}$ derived from FD-$LaCoO_3$ proceeds slowly, as a result of which these oxides are detected by *ex situ* XRD experiments. The recovering of the FD-$LaCoO_3$ composition is achieved by heating the reduced oxides at 100 °C in air for 2 h (not shown). These results show that the lower the reduction stability of $LaCoO_3$; the higher the oxygen ability of its reduced product. By increasing the annealing temperature, as well as by using the freeze-dried citrates instead of Pechini-type precursors, the reduction reaction of $LaCoO_3$ at the initial stage is divided into the formation of Brownmillerite-type oxides and Co metal. The appearance of Co metal and the Ruddlesden–Popper phases $La_{m+1}Co_mO_{3m+1}$ contributes, on its turn, to the increase in temperature of the final reduction to Co metal and La_2O_3.

4. Conclusions

The formation of $LaCoO_3$ perovskites starts at 400 °C by the reaction between $La_2O_2CO_3$ and a Co-spinel phase after the decomposition of the organic components. Further annealing at 600 °C yields well-crystallized $LaCoO_3$ with excess of oxygen when freeze-dried La–Co-citrates are used as precursors, while $LaCoO_3$ with a slight oxygen deficiency is obtained by the Pechini method. A lower organic content in the precursor gives rise to the stabilization of structural defects comprising highly oxidized ferromagnetic coupled Co ions (such as Co^{4+}). The type of the citrate precursor affects the powder morphology: plate-like aggregates are obtained from freeze-dried citrates, while loosely bonded particles are formed by the Pechini method. The different morphology is a consequence of the thermal properties of precursors: the decomposition of the Pechini-type precursors is accompanied by the deposition of carbon, which burns exothermally at temperatures above 400 °C. Inside the aggregates, nanometric hexagonal individual particles are observed, the particle dimensions being insensitive towards the organic components in the precursors (60–80 nm). With increase in annealing temperature, the crystallite growth is favored for P-$LaCoO_3$.

The complete reduction of $LaCoO_3$ with H_2 proceeds to Co metal and La_2O_3. The synthesis procedure has a strong impact on the intermediate stage of $LaCoO_3$ reduction. For an oxide obtained by the Pechini method, the reduction of Co^{3+} ions is completed via the formation of Brownmillerite-type phases ($La_nCo_nO_{3n-1}$), while for the oxides obtained from freeze-dried citrates, oxygen-deficient phases together with Co metal are formed. By increasing the annealing temperature, the formation of Co metal and Ruddlesden–Popper-type oxides as intermediate reduction products become more significant. The appearance of Ruddlesden–Popper phases and Co metal leads to an increase in temperature of the final reduction to Co metal and La_2O_3.

Acknowledgments

Authors are grateful to EC for a grant within the FAME project (FAME FP6-500159-1) and to the Centre of Competence MISSION (SSA, EC-INCO-CT-2005-016414). Authors are grateful to the financial support from the National Science Fund of Bulgaria (IDEAS No D002-309/2008).

References

[1] S.M. Haile, Acta Materialia 51 (2003) 5981–6000.

[2] Frank de Bruijn, Green Chem. 7 (2005) 132–150.
[3] H. Tanaka, M. Misono, Curr. Opin. Solid State Mater. Sci. 5 (2001) 381–387.
[4] T. Nitadori, S. Kurihashi, M. Misono, J. Catal. 98 (1986) 221.
[5] S. Nakayama, M. Okazaki, Y.L. Aung, M. Sakamoto, Solid State Ionics 158 (2003) 133.
[6] M.A. Senaris-Rodrigues, J.B. Goodenough, J. Solid State Chem. 116 (1995) 224.
[7] M. Wallin, N. Cruise, U. Klement, A. Palmqvist, M. Skoglundh, Colloids Surf. A 238 (2004) 27.
[8] M. Popa, M. Kakihana, Solid State Ionics 151 (2002) 251.
[9] M. Popa, J. Franti, M. Kakihana, Solid State Ionics 154–155 (2002) 135.
[10] H.-J. Kweon, D.G. Park, S.-T. Kuk, H.-B. Park, K. Kim, Bull. Korean Chem. Soc. 18 (1997) 1249.
[11] H. Taguchi, H. Yoshioka, M. Nagao, J. Mater. Sci. Lett. 13 (1994) 891.
[12] H. Taguchi, S. Yamada, M. Nagao, Y. Ichikawa, K. Tabata, Mater. Res. Bull. 37 (2002) 69.
[13] Y. Zhu, R. Tan, T. Yi, S. Ji, X. Ye, L. Cao, J. Mater. Sci. 35 (2000) 5415.
[14] S. Sundar Manoharan, K.C. Patil, J. Solid State Chem. 102 (1993) 267.
[15] V.V. Kharton, F.M. Figueirido, A.V. Kovalevski, A.P. Viskup, E.N. Naumovich, A.A. Yaremchenko, I.A. Bashmakov, F.M.B. Marques, J. Eur. Ceram. Soc. 21 (2001) 2301.
[16] D. Berger, C. Matei, F. Papa, G. Voicu, V. Fruth, Progr. Solid State Chem. 35 (2007) 183.
[17] F. Deganello, G. Marcì, G. Deganello, J. Eur. Ceram. Soc. 29 (2009) 439.
[18] T. Ito, Q. Zhang, F. Saito, Powder Technol. 143–144 (2004) 170.
[19] Y. Wang, X. Yang, L. Lu, X. Wang, Thermochim. Acta 443 (2006) 239.
[20] M.P. Pechini, US Patent No 3,330,697 (1967).
[21] M. Kakihana, J. Sol–Gel Sci. Technol. 6 (1996) 7.
[22] A. Worayingyong, P. Kangvansura, S. Ausadasuk, P. Praserthdam, Colloids Surf. A 315 (2008) 217.
[23] A. Gaki, O. Anagnostaki, D. Kioupis, T. Perraki, D. Gakis, G. Kakali, J. Alloys Compd. 451 (2008) 305.
[24] A. Mai, F. Tietz, D. Stöver, Solid State Ionics 173 (2004) 35.
[25] F. Tietz, A. Mai, D. Stöver, Solid State Ionics 179 (2008) 1509.
[26] A. Boreave, H. Tan, V. Roche, Ph. Vernoux, J.P. Deloume, Solid State Ionics 179 (2008) 1071.
[27] T. Nakamura, G. Petzov, L.J. Gauckler, Mater. Res. Bull. 14 (1979) 649.
[28] M. Crespin, W.K. Hall, J. Catal. 69 (1981) 359.
[29] M. Radovic, S.A. Speakman, L.F. Allard, E.A. Payzant, E. Lara-Curzio, W.M. Kriven, J. Lloyd, L. Fegely, N. Orlovskaya, J. Power Sources 184 (2008) 77.
[30] L.B. Sis, G.P. Wirtz, S.C. Sorenson, J. Appl. Phys. 44 (1973) 5553.
[31] L. Huang, M. Bassir, S. Kaliaguine, Appl. Surf. Sci. 243 (2005) 360.
[32] E.A. Lombardo, K. Tanaka, I. Toyoshima, J. Catal. 80 (1983) 340 (XPS).
[33] J.A. Marcos, R.H. Buitrago, E.A. Lombardo, J. Catal. 105 (1987) 95.
[34] S. Royer, F. Bérubé, S. Kaliagiune, Appl. Catal. A 282 (2005) 273.
[35] S. Ivanova, E. Zhecheva, R. Stoyanova, J. Phys. Chem. Solids 68 (2007) 168.
[36] M.M. Natile, E. Ugel, Ch. Maccato, A. Glisenti, Appl. Catal. 72 (2007) 351.
[37] V.V. Kharton, F.M. Figueiredo, A.V. Kovalevsky, A.P. Viskup, E.N. Naumovich, A.A. Yaremchenko, I.A. Bashmakov, F.M.B. Marques, J. Eur. Ceram. Soc. 21 (2001) 2301.
[38] L. Armelao, G. Bandoli, D. Barreca, M. Bettinelli, G. Bottaro, A. Caneschi, Surf. Interface Anal. 34 (2002) 112.
[39] C. Oliva, S. Cappelli, A. Kryukov, G.L. Chiarello, A.V. Vishniakov, L. Forni, J. Mol. Catal. A: Chem. 247 (2006) 248.
[40] T. Roisnel, J. Rodriguez-Carvajal, Mater. Sci Forum 378–381 (2001) 118.
[41] D. Hennings, W. Mayr, J. Solid State Chem. 26 (1978) 329.
[42] R. Robert, L. Bocher, B. Sipos, M. Döbeli, A. Weidenkaff, Prog. Solid State Chem. 35 (2007) 447.
[43] E. Zhecheva, R. Stoyanova, M. Gorova, R. Alcantara, J. Morales, J.-L. Tirado, Chem. Mater. 8 (1996) 1429.
[44] R. Alcantara, P. Lavela, J.-L. Tirado, R. Stoyanova, E. Kuzmanova, E. Zhecheva, Chem. Mater. 9 (1997) 2145.
[45] N. Petrova, D. Todorovsky, Mater. Res. Bull. 41 (2006) 576.
[46] M.M. Milanova, M.G. Arnaudov, M.M. Getsova, D.S. Todorovsky, J. Alloys Compd. 264 (1998) 95.
[47] O. Haas, R.P. Struis, J.M. McBreen, J. Solid State Chem. 177 (2004) 1000.
[48] G. Thornton, B.C. Tofield, A.W. Hewat, J. Solid State Chem. 61 (1986) 301.
[49] S. Ivanova, E. Zhecheva, R. Stoyanova, Phys. Stat. Sol. A 205 (2008) 1685.
[50] R.D. Shannon, C.T. Prewitt, Acta Cryst. B25 (1969) 925.
[51] O.H. Hansteen, H. Fjellvåg, B.C. Hauback, J. Mater. Chem. 8 (1998) 2081.
[52] K. Vidyasagar, A. Reller, J. Gopalakrishnan, C.N.R. Rao, J. Chem. Soc., Chem. Commun. (1985) 7.
[53] B. Gilbu Tilset, H. Fjellvåg, A. Kjekshus, J. Solid State Chem. 119 (1995) 271.
[54] G.L. Charello, J.-D. Grunwald, D. Ferri, F. Krumeich, C. Oliva, L. Forni, A. Baiker, J. Catal. 252 (2007) 127.
[55] M. Seppänen, M. Kytö, P. Taskinen, Scand. J. Metall. 8 (1979) 199.
[56] B. Sextory, A. Hughes, T. Turney, J. Catal. 97 (1986) 390.
[57] E. Manova, T. Tsoncheva, Cl. Estournès, D. Paneva, K. Tenchev, I. Mitov, L. Petrov, Appl. Catal. A 300 (2006) 170.
[58] N.A. Merino, B.P. Barbero, P. Grange, L.E. Cadús, J. Catal. 231 (2005) 232.
[59] G. Valderrama, A. Kiennemann, M.R. Goldwasser, Catal. Today 133–135 (2008) 142.